CHEMISTRY
A EUROPEAN JOURNAL

FULL PAPER

DOI: 10.1002/chem.201200880

Direct Detection of Key Intermediates in Rhodium(I)-Catalyzed [2+2+2] Cycloadditions of Alkynes by ESI-MS

Magda Parera,[a] Anna Dachs,[a, b] Miquel Solà,[a, b] Anna Pla-Quintana,*[a] and Anna Roglans*[a]

Abstract: The mechanism of the Rh-catalysed [2+2+2] cycloaddition reaction of diynes with monoynes has been examined using ESI-MS and ESI-CID-MS analysis. The catalytic system used consisted of the combination of a cationic rhodium(I) complex with bisphosphine ligands, which generates highly active complexes that can be detected by ESI(+) experiments. ESI-MS online monitoring has allowed the detection for the first time of all of the intermediates in the catalytic cycle, supporting the mechanistic proposal based mainly on theoretical calculations. For all ESI-MS experiments, the structural assignments of ions are supported by tandem mass spectrometry analyses. Computer model studies based on density functional theory (DFT) support the structural proposal made for the monoyne insertion intermediate. The collective studies provide new insight into the reactivity of cationic rhodacyclopentadienes, which should facilitate the design of related rhodium-catalysed C–C couplings.

Keywords: cycloaddition · density functional calculations · electrospray ionization · mass spectrometry · rhodium

Introduction

Given the importance of transition-metal-catalysed reactions in organic synthesis, it is of great interest to understand the reaction mechanisms to be able to improve these processes. One of the difficulties faced in these investigations is that due to the low concentrations and transient nature of most of the intermediates involved, the identification of the species is complex and limited information is obtained. Therefore, techniques that allow the direct monitoring of these reactive intermediates are of great interest. One such method is electrospray ionization mass spectrometry (ESI-MS),[1] which makes it possible to obtain detailed data by trapping and identifying short-lived intermediates in organometallic catalytic cycles in a relatively simple manner.[2] In addition to revealing the molecular masses of ions for many reactive intermediates, this technique also provides structural information through characteristic fragmentation patterns obtained by collision-induced dissociation (CID).

Although many transition-metal-catalysed reactions have already been studied using ESI-MS,[2–4] to the best of our knowledge the metal-catalysed [2+2+2] cycloaddition reaction has never been analysed in this way. The generally accepted reaction mechanism for this cycloaddition involving three alkynes is shown in Scheme 1.

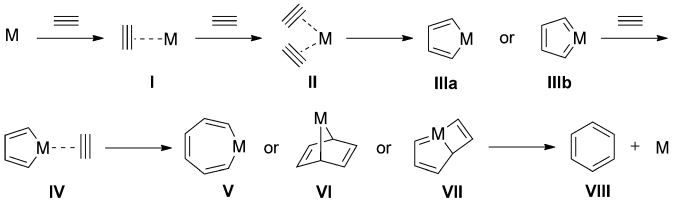

Scheme 1. Mechanistic proposal for [2+2+2] cycloaddition reactions of three alkynes.

Initially, one alkyne moiety displaces a ligand on the metal to form alkyne complex **I**, and then a second alkyne coordinates to form complex **II**. Oxidative coupling may occur to give a metallacyclopentadiene **IIIa** or a metallacyclopentatriene **IIIb**, in which the metal adopts a formal oxidation state two units higher than that in the precursor **II**. This has been found to be the rate-determining step, with activation energies typically in the range of 11–14 kcal mol^{-1}. Subsequent coordination of a third alkyne ligand to the metallacyclopentadiene or metallacyclopentatriene intermediate is followed either by alkyne insertion to form a metallacycloheptatriene **V** (the so-called Schore's mechanism)[5] or metal-mediated [4+2] cycloaddition to yield a 7-metallanorbornadiene complex **VI** or cycloaddition to give a metallabicyclo[3.2.0]heptatriene **VII**. Finally, the arene is formed by reductive elimination of the metal and the catalyst (M) is recovered. Although this is the general pattern of the reaction mechanism, the specific nature of the inter-

[a] M. Parera, Dr. A. Dachs, Prof. Dr. M. Solà, Dr. A. Pla-Quintana, Prof. Dr. A. Roglans
Departament de Química, Universitat de Girona
Campus de Montilivi, s/n, 17071 Girona (Spain)
E-mail: anna.plaq@udg.edu
anna.roglans@udg.edu

[b] Dr. A. Dachs, Prof. Dr. M. Solà
Institut de Química Computacional, Universitat de Girona
Campus de Montilivi, s/n, 17071 Girona (Spain)

Supporting information for this article is available on the WWW under http://dx.doi.org/10.1002/chem.201200880.

mediates in each process depends on the nature of the metal, the ligands, and even the substrate partners. The mechanistic proposal in Scheme 1 is essentially based on theoretical calculations[6] and only limited experimental data are available to support the proposed overall mechanism. Although several metallacyclopentadiene and metallacyclopentatriene intermediates have been isolated, to the best of our knowledge there are no experimental data relating to more advanced intermediates in the catalytic cycle.

Among the several transition metals able to catalyse the [2+2+2] cycloaddition reaction, rhodium is becoming increasingly popular, which has led to considerable interest in studying the particularities of the mechanism for reactions involving this metal. Several studies have dealt with the characterization of rhodacyclopentadienes of type **IIIa** (Scheme 1), the intermediate that is commonly proposed in rhodium-catalysed [2+2+2] cycloadditions, by means of techniques such as NMR and IR spectroscopies and X-ray analysis.[7] ESI-MS has been used a limited number of times to detect rhodacyclopentadienes in on-going reactions, mainly by our group[4j,k] but also in a recent paper by Brodbelt, Baik, Krische et al.,[8] which was concerned with the mechanism of the hydrogen-mediated coupling of acetylenes, a reaction that shares the first steps of the catalytic cycle with the [2+2+2] cycloaddition of alkynes. Furthermore, during our continuing study of [2+2+2] cycloaddition reactions catalysed by rhodium complexes,[4j,k,9] in which a contribution has been made to the understanding of mechanistic aspects by theoretical approaches,[6k,l] we have also reported kinetic data for the catalytic cycle of an [RhCl(PPh$_3$)$_3$]-catalysed [2+2+2] cycloaddition of bisalkynes with a monoalkyne, following the reaction by means of electrochemical techniques to study the successive steps separately.[4k]

In this study, we present the first ESI-MS investigation of [2+2+2] cycloaddition reactions between several diynes and monoalkynes catalysed by Rh^{I}. In addition, density functional theory (DFT) calculations have been used to help in the identification of the structures of some of the intermediates detected by ESI-MS.

Results and Discussion

Our group has previously used the Wilkinson catalyst both in methodological studies and in the characterization of oxidative addition intermediates by ESI-MS.[4k] However, the neutral rhodium-containing species postulated to be formed are undetectable by ESI-MS and there must be an ionization mechanism operating in order for them to be detected. Chloride dissociation allowed us to detect the oxidative addition intermediate when using Wilkinson's catalyst, but no further intermediate could be detected. We therefore decided to use a cationic Rh^{I} complex to facilitate the observation of ionic species by ESI-MS. The combination of [Rh(cod)$_2$]BF$_4$ (cod = cyclooctadiene) with BINAP-type (BINAP = 2,2′-bis(diphenylphosphino)-1,1′-binaphthyl) ligands has been shown to be an efficient catalyst for [2+2+2] cycloaddition reactions[10] and was therefore the catalytic system of choice. Our mechanistic study commenced with the cycloaddition of diyne **1** and *p*-methylphenylacetylene **2a** (Scheme 2). The reaction was first optimized in the laboratory and quantitatively afforded cycloadduct **3a** after 2 h in refluxing dichloroethane.

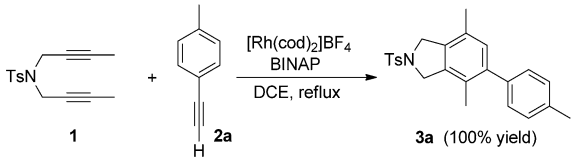

Scheme 2. [2+2+2] Cycloaddition reaction between diyne **1** and *p*-methylphenylacetylene **2a** studied by ESI-MS.

To determine the sensitivity of the technique towards the species present in the reaction mixture, the first step was to individually analyse the components of the reaction by ESI-MS. All of the species detected in the present study were assigned by comparison of the experimentally obtained isotopic pattern and the theoretically calculated one (see the Supporting Information). The behaviours of the starting diyne **1** and final product **3** were examined, both of which afforded peaks corresponding to the $[M+H]^+$ and $[M+Na]^+$ adducts. The components of the catalytic system were then analysed. [Rh(cod)$_2$]BF$_4$ was dissolved in MeOH and injected into the mass spectrometer. One peak was observed at $m/z = 211.0$, corresponding to the complex $[Rh(cod)]^+$ that had lost a cod ligand. Analysis of the BINAP ligand by ESI-MS gave the molecular peak $[BINAP+H]^+$ at $m/z = 623.2$, but the peak of an oxidized species $[BINAP{=}O+H]^+$ was also observed at $m/z = 639.2$. This oxidized species could be formed in the same mass spectrometer since an oxidative positive ESI mode was used and the presence of traces of oxygen was possible given the purity of the nebulizing nitrogen employed. The active catalytic species was then generated by hydrogenating[11] a 1:1 mixture of [Rh(cod)$_2$]BF$_4$ and the BINAP ligand in dichloromethane, and, following dilution with MeOH,[12] this mixture was analysed by ESI-MS. The spectrum showed the species $[Rh(BINAP)]^+$ at $m/z = 725.1$, $[Rh(cod)BINAP]^+$ at $m/z = 833.1$, and $[Rh(BINAP)_2]^+$ at $m/z = 1347.0$. The peak at $m/z = 833.1$ was fragmented by CID, resulting in loss of the cod ligand and leading to the formation of $[Rh(BINAP)]^+$ at $m/z = 725.0$.

The complete reaction resulting from the addition of diyne **1** to the mixture of hydrogenated [Rh(cod)$_2$]BF$_4$ and BINAP together with 1.5 equivalents of *p*-methylphenylacetylene **2a** in dichloroethane was the next mixture to be analysed by ESI-MS. After heating at reflux for 15 min in an inert atmosphere, a sample was diluted in MeOH[12] and injected into the mass spectrometer (Figure 1a). The postulated catalytically active species $[Rh(BINAP)]^+$ was detected at $m/z = 725.2$. The peak observed at $m/z = 1000.3$ corresponds to the mass of a cluster containing [Rh-

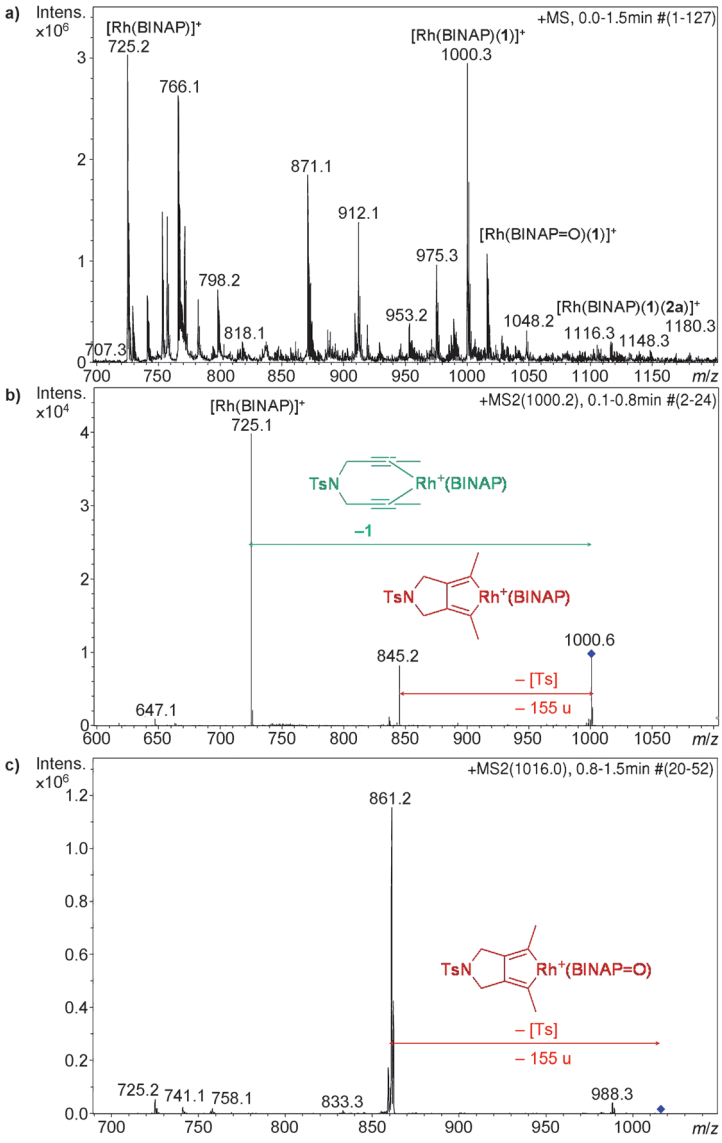

Figure 1. a) ESI mass spectrum of a mixture of ($[Rh(cod)_2]BF_4$ + BINAP) (5 mol%) + **2a** + **1** after 15 min. b) CID mass spectrum of the ion at $m/z = 1000.3$. c) CID mass spectrum of the ion at $m/z = 1016.3$.

(BINAP)(**1**)]$^+$. Since the peak may correspond to two possible intermediates, one resulting from the coordination of the diyne to rhodium (species of type **II** in Scheme 1) and the other resulting from oxidative addition of the diyne to the metal (species of type **IIIa** in Scheme 1), we further characterized them by conducting an MS/MS analysis (Figure 1b). The peak at $m/z = 1000.3$ suffered fragmentation resulting in a peak at $m/z = 725.0$, corresponding to the fragment [Rh(BINAP)]$^+$, which was further cleaved to release a fragment $[M-155]^+$ corresponding to loss of the tosyl group. Had the insertion step already occurred, [Rh(BINAP)]$^+$ would not have been observed because the insertion step is effectively irreversible.[8] Therefore, we assign the cluster at $m/z = 1000.3$ to a mixture of the two intermediates: the coordination intermediate fragmenting to [Rh(BINAP)]$^+$ by dissociation of the diyne component from the metal, and the oxidative addition intermediate fragmenting by tosyl loss through S–N bond fragmentation, a common fragmentation suffered by aryl sulfonamides in mass spectrometry.[13] A peak was also observed in the reaction mixture at $m/z = 1016.3$ attributable to the species [Rh(BINAP=O)(**1**)]$^+$. MS/MS studies of this compound (Figure 1c) indicated that it was cleaved to release a fragment $[M-155]^+$ corresponding to loss of the tosyl group, from which we concluded that it corresponds to the oxidized form of the oxidative addition intermediate.

The oxidative addition is thought to be the rate-determining step of the [2+2+2] cycloaddition reaction. The ensuing intermediates might therefore be present at very low concentrations, such that they are likely to be detected, if at all, as minor ions. In the search for these minor ions, spectra were expanded paying special attention to the m/z 1110–1120 region. We were delighted to observe a small peak at $m/z = 1116.3$, corresponding to the formal addition of *p*-methylphenylacetylene to the intermediate [Rh(BINAP)(**1**)]$^+$. This peak may also correspond to different intermediates: one involving π-coordination of acetylene **2a** to rhodacyclopentadiene, another resulting from alkyne insertion into the same intermediate, or a third being a coordination species of the final product **3a** with the catalyst. Given the importance of the observation of the peak at $m/z = 1116.3$, we proceeded to further characterize the nature of this intermediate by MS/MS (Figure 2a). If the insertion step had not occurred, fragmentation would have

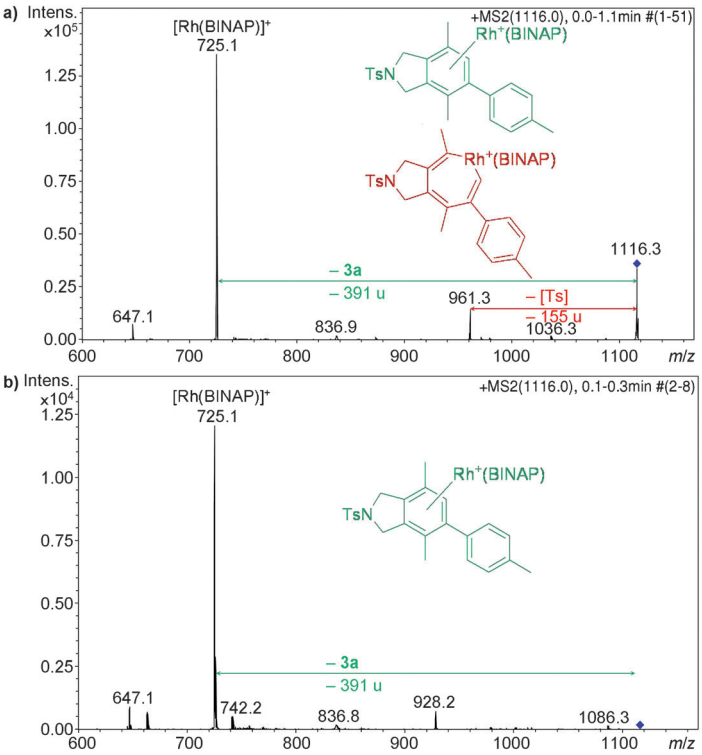

Figure 2. a) CID mass spectrum of the ion at $m/z = 1116.3$ at a collision energy of 0.95 V. b) CID mass spectrum of the ion at $m/z = 1115.9$ at a collision energy of 0.95 V originating from a mixture of **3a** + Rh catalyst.

caused simple *p*-methylphenylacetylene dissociation and the formation of a fragment at $m/z = 1000.3$. Since this was not observed, a π-coordination intermediate can be ruled out. In fact, two main fragments arose after CID of the peak at $m/z = 1116.3$, one at $m/z = 961.3$ corresponding to loss of the tosyl group, and another at $m/z = 725.1$ corresponding to the mass of $[Rh(BINAP)]^+$. This last fragment was derived from the loss of 391 mass units, exactly the weight of the final product **3a**. Whereas the formation of $[Rh(BINAP)]^+$ may be the result of either reductive elimination from the insertion intermediate or product dissociation from the complex formed by coordination of the catalyst to the final product, the tosyl group is presumably lost from the oxidative insertion intermediate. Further evidence for this was gained by injecting into the mass spectrometer a mixture of **3a** in dichloroethane and 5 mol% of the catalytic mixture diluted with MeOH. The catalytic mixture gave the three peaks that have already been mentioned ($[Rh(BINAP)]^+$ at $m/z = 725.1$, $[Rh(cod)BINAP]^+$ at $m/z = 833.1$, and $[Rh(BINAP)_2]^+$ at $m/z = 1347.0$) and upon addition of the final product **3a**, coordination of **3a** to the catalytic species $[Rh(BINAP)]^+$ was observed as a peak at $m/z = 1115.9$. When this peak was submitted to CID at the same collision energy as in the previous experiment, it only gave the $[Rh(BINAP)]^+$ fragment at $m/z = 725.1$ without loss of the tosyl group (compare spectra a and b, Figure 2).[14] We therefore conclude that we have detected for the first time the addition intermediate.

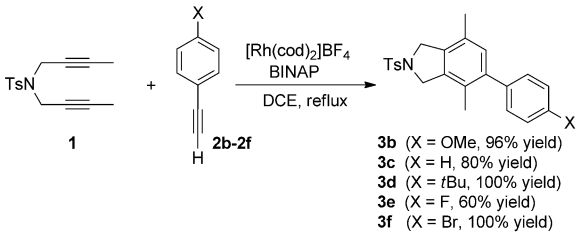

Scheme 3. [2+2+2] Cycloaddition reactions between diyne **1** and *p*-X-phenylacetylenes **2b–f** studied by ESI-MS.

Table 1. Electrospray mass spectral data for reactions described in Scheme 3.

Entry	Monoyne **2**/X	MS $[m/z]$/identified species	MS/MS $[m/z]$/identified species
1	**2b**/OMe	1132.2/$[Rh(BINAP)(\mathbf{1})(\mathbf{2b})]^+$	977.0 $[Rh(BINAP)(\mathbf{1})(\mathbf{2b})-Ts]^+$ 725.0 $[Rh(BINAP)]^+$
2	**2c**/H	1101.9/$[Rh(BINAP)(\mathbf{1})(\mathbf{2c})]^+$	946.9 $[Rh(BINAP)(\mathbf{1})(\mathbf{2c})-Ts]^+$ 725.0 $[Rh(BINAP)]^+$
3	**2d**/*t*Bu	1158.3/$[Rh(BINAP)(\mathbf{1})(\mathbf{2d})]^+$	1003.3 $[Rh(BINAP)(\mathbf{1})(\mathbf{2d})-Ts]^+$ 725.1 $[Rh(BINAP)]^+$
4	**2e**/F	1120.2/$[Rh(BINAP)(\mathbf{1})(\mathbf{2e})]^+$	964.9 $[Rh(BINAP)(\mathbf{1})(\mathbf{2e})-Ts]^+$ 724.9 $[Rh(BINAP)]^+$
5	**2f**/Br	1180.2–1182.2/$[Rh(BINAP)(\mathbf{1})(\mathbf{2f})]^+$	1026.8 $[Rh(BINAP)(\mathbf{1})(\mathbf{2f})-Ts]^+$ 724.9 $[Rh(BINAP)]^+$

The reaction was monitored at fixed time intervals by ESI-MS. The reaction was complete after 2 h (TLC monitoring) and we were able to observe the disappearance of the ions corresponding to the intermediates at $m/z = 1000$ (oxidative addition) and $m/z = 1116$ (insertion) and the formation of the final product **3a** (see the Supporting Information for spectra).

To confirm the species detected and to test the general applicability of the method, we studied the cycloaddition reaction by varying the nature of the monoalkyne. Cycloaddition reactions with a series of *para*-substituted phenylacetylenes **2b–f** (Scheme 3 and Table 1) with the same tosyl-tethered diyne **1** were analysed. The new reactions analysed by ESI-MS, under reaction conditions previously optimized in the laboratory, are shown in Scheme 3.

When the reactions were studied by ESI-MS following the same methodology as before, data analogous to the results with *p*-methylphenylacetylene were obtained, confirming our initial assignments. In Table 1, only the clusters corresponding to the second intermediate and their further characterization by MS/MS are shown in detail as the oxidative addition intermediate is the same in all the examples. In all cases, the MS/MS experiments showed both the loss of tosyl groups and, by dissociation of the final product from the catalyst or by the reductive elimination process from the alkyne insertion intermediate, formation of the $[Rh(BINAP)]^+$ fragment at $m/z = 725.0$. To confirm the detection of the alkyne insertion intermediate and to exclude the mere formation of a species corresponding to coordination of the catalyst to the final product, a mixture of **3d** and 5 mol% $[Rh(cod)_2]BF_4$ and BINAP was analysed. The spectrum showed a peak at $m/z = 1158.0$ corresponding to the coordination species, but when this peak was submitted to MS/MS only a fragment at $m/z = 725.0$ was observed. No loss of the tosyl group was seen in this case either (see the Supporting Information), confirming the observation of the alkyne insertion intermediate in the ensuing reactions.

We then studied the effect of variation of the diyne and performed the reaction with an NTs-tethered terminal diyne **4** and phenylacetylene **2c** (Scheme 4 and Table 2).

The starting diyne **4** and the final product **5** were individually injected into the mass spectrometer for analysis. Both were detected as protonated species or sodium adducts. In the case of diyne **4** and cycloadduct **5**, MS/MS experiments showed Ts loss but as a neutral molecule resulting from heterolytic cleavage.[15] This differs from the behaviour of the

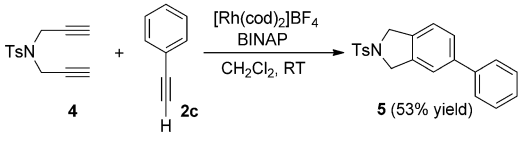

Scheme 4. [2+2+2] Cycloaddition reaction between diyne **4** and phenylacetylene **2c** studied by ESI-MS.

Table 2. Electrospray mass spectral data for mixtures of reactions in Scheme 4 in MeOH.

Sample[a]	MS [m/z]/identified species	MS/MS [m/z]/identified species
$[Rh(cod)_2]BF_4$+BINAP+**4**+**2c**	972.1/$[Rh(BINAP)(\mathbf{4})]^+$	816.9 $[Rh(BINAP)(\mathbf{4})-Ts]^+$ 725.1 $[Rh(BINAP)]^+$
	988.1/$[Rh(BINAP{=}O)(\mathbf{4})]^+$	833.1 $[Rh(BINAP{=}O)(\mathbf{4})-Ts]^+$
	1074.1/$[Rh(BINAP)(\mathbf{4})(\mathbf{2c})]^+$	919.1 $[Rh(BINAP)(\mathbf{4})(\mathbf{2c})-Ts]^+$ 724.9 $[Rh(BINAP)]^+$
	1218.9/$[Rh(BINAP)(\mathbf{4})_2]^+$	1063.9 $[Rh(BINAP)(\mathbf{4})_2-Ts]^+$
$[Rh(cod)_2]BF_4$+BINAP+**5**	1074.3/$[Rh(BINAP)(\mathbf{5})]^+$	725.1 $[Rh(BINAP)]^+$

[a] 5 mol% of rhodium complex and bisphosphine was used.

previously observed intrinsically ionic rhodium intermediates, in which homolytic cleavage led to the loss of radical Ts and the detection of a cationic radical fragment (Scheme 5).[13]

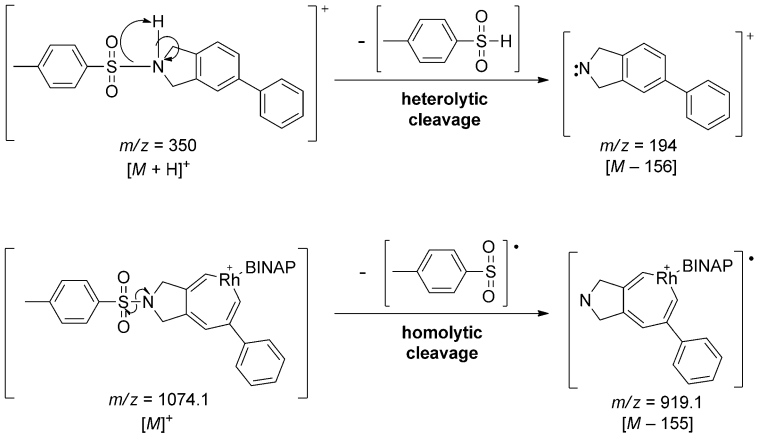

Scheme 5. Homolytic versus heterolytic cleavage of tosyl-containing species.

The solution resulting from the reaction between *N*-tosyl diyne **4** and phenylacetylene **2c** was injected into the mass spectrometer after 15 min of reaction at room temperature and dilution with MeOH. Intermediates analogous to those detected for *N*-tosyl diyne **1** were observed and found to display similar behaviour in the fragmentation experiments with CID (Table 2; for mass spectra, see the Supporting Information) with the exception of the observation of a new cluster at $m/z=1218.9$ corresponding to the mass of $[Rh(BINAP)(\mathbf{4})_2]^+$. This cluster can be assigned either to insertion of a second molecule of *N*-tosyl diyne **4** into the oxidative addition intermediate (an intermediate that led to the homo-coupling of *N*-tosyl diyne **4**) or to complexation of the catalyst with the homo-coupled product. ESI-MS/MS analysis showed only a loss of the Ts group, which indicates that it corresponds to the addition rather than the coordination intermediate. The fact that terminal alkynes are more prone to homo-coupling than their non-terminal counterparts may explain why these intermediates were exclusively observed in this set of experiments.

To characterize in depth the nature of the species detected at $m/z=972$, a series of experiments was run to study the dependence of fragment yields on the collision energy (Figure 3). We hypothesized that this species was a mixture of the diyne coordinated to the catalyst and the oxidative addition intermediate, each one fragmenting through a characteristic pathway. This was corroborated by the present study, since the fragmentation of non-covalent bonds (i.e., diyne dissociation from the catalyst leading to the catalyst fragment at $m/z=725$) starts to take place at lower amplitudes ($A>0.15$) than the fragmentation of covalent bonds ($A>0.17$) (tosyl cleavage from the oxidative coupling intermediate leading to the fragment at $m/z=817$). The breaking of coordination bonds occurs to a much greater extent than the breaking of the N–Ts covalent bond throughout the collision energy range studied. Furthermore, on increasing the collision energy, the difference in the relative abundances of the two fragments (725 vs. 817) is increased. We rule out the possibility that the fragment at $m/z=817$ originates from the coordination intermediate, since the dissociation of non-covalent bonds should be much more favourable than the breaking of a covalent bond.

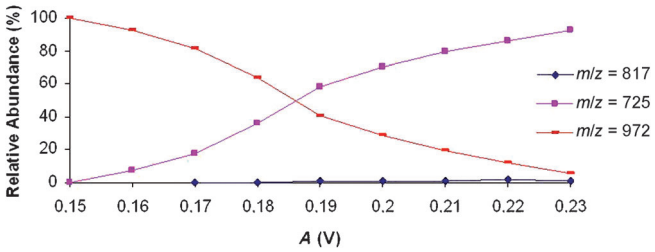

Figure 3. Study of the dependence of fragment yields on the collision energy at a reaction time of 45 min.

In line with the study of the variation of the diyne reagent, we performed a second experiment using a malonate-tethered diyne to obtain a different fragmentation pattern of the reaction products and intermediates. The reaction between diyne **6** and *p*-methylphenylacetylene **2a**, performed in the laboratory, gave a 50% yield of cycloadduct **7** (Scheme 6).

Cycloadduct **7** was injected into the ESI-MS apparatus and gave an adduct at $m/z=353.0$ corresponding to $[M+H]^+$, which underwent CID fragmentation to give a peak at $m/z=325.0$ arising from a McLafferty rearrange-

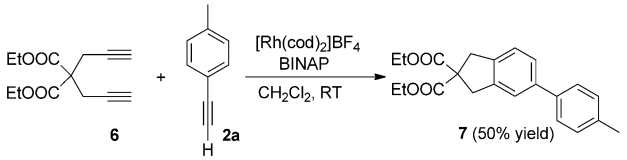

Scheme 6. [2+2+2] Cycloaddition reaction between malonate-tethered diyne **6** and *p*-methylphenylacetylene **2a** studied by ESI-MS.

ment ($[\mathbf{7}-C_2H_4]^+$), and another peak at $m/z=325.0$ resulting from the loss of COOEt and H. The ensuing reaction was then analysed under the standard conditions. Apart from the species $[Rh(BINAP)(cod)]^+$ at $m/z=833.3$ and $[Rh(BINAP)_2]^+$ at $m/z=1347.3$ that were assigned to the catalytic system, new signals appeared relating to intermediates in the reaction. In the m/z 960–980 region, in which peaks due to oxidative addition intermediates were expected, a peak at $m/z=977.3$ was assigned to $[Rh(BINAP{=}O)(\mathbf{6})]^+$. CID fragmentation of this compound showed the formation of a peak at $[M-73]^+$ (Figure 4a), corresponding to the loss of a COOEt group, which indicated that the cluster at $m/z=977.3$ corresponded to the oxidized form of the oxidative addition intermediate and not to a coordination species. Only a small peak was observed at $m/z=961.3$ corresponding to $[Rh(BINAP)(\mathbf{6})]^+$, the low intensity of which prevented full isolation and fragmentation. The mass region corresponding to the alkyne insertion intermediate was then analysed. A peak at $m/z=1077.3$ was observed, which could be assigned to a cluster incorporating both the diyne and monoyne, $[Rh(BINAP)(\mathbf{6})(\mathbf{2a})]^+$. MS/MS analysis of this peak was performed, as a result of which it was assigned to monoyne coordination to the oxidative addition intermediate, the alkyne insertion intermediate, or the coordination of the cycloadduct **7** to the catalyst. The main fragment at $m/z=725.1$ corresponded to $[Rh(BINAP)]^+$, which indicated the presence of a species involving coordination of cycloadduct **7** to the catalyst, although we cannot rule out the possibility that it was formed through reductive elimination from the alkyne insertion intermediate. A peak attributable to $[Rh(BINAP{=}O)(\mathbf{6})(\mathbf{2a})]^+$ was also observed at $m/z=$ 1093.3. CID analysis revealed two main peaks (Figure 4b). The first fragment at $m/z=741.1$ corresponded to $[Rh(BINAP{=}O)]^+$ and, analogously to the peak of the non-oxidized species, indicated the presence of the latter intermediate involving coordination of the cycloadduct **7** to the catalyst, although it could possibly also have been formed from the alkyne insertion intermediate. However, unlike the peak of the non-oxidized species, a fragment attributable to $[Rh(BINAP{=}O)(\mathbf{6})]^+$ was observed at $m/z=977.2$. The formation of this fragment indicated the presence of an intermediate in which monoyne **2a** was coordinated to the oxidative addition intermediate, which fragmented by dissociation of the metal from the monoyne. We can therefore conclude that we also observed the hitherto elusive intermediate of coordination of the monoyne to the oxidative addition intermediate. Given that diyne **6** bears terminal alkyne moieties, intermediates leading to the homo-coupled products were also observed at $m/z=1197.0$, assigned to $[Rh(BINAP)(\mathbf{6})_2]^+$, and at $m/z=1213.4$, assigned to $[Rh(BINAP{=}O)(\mathbf{6})_2]^+$. Both fragmented by dissociation of the homo-coupled product from the ligand or reductive elimination to give $[Rh(BINAP)]^+$ and $[Rh(BINAP{=}O)]^+$, respectively.[16]

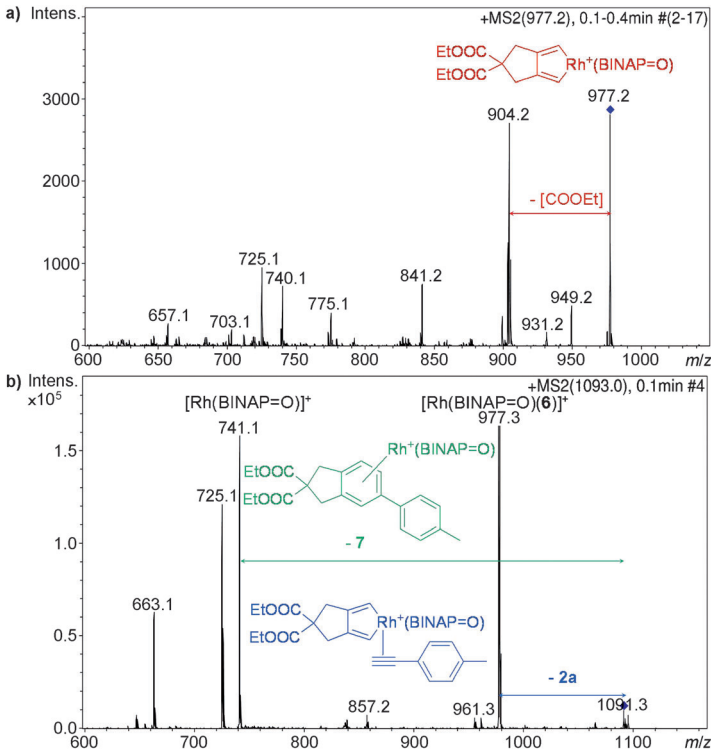

Figure 4. a) CID mass spectrum of the ion at $m/z=977.3$. b) CID mass spectrum of the ion at $m/z=1093.3$ showing the dissociation of the metal from the monoyne.

After varying the monoyne and diyne reactants, a third set of experiments was conducted on the cycloaddition of diyne **4** and phenylacetylene **2c** (reaction in Scheme 4) with different bisphosphines, (*R*)-H_8-BINAP (H_8-BINAP = 2,2′-bis(diphenylphosphino)-5,5′,6,6′,7,7′,8,8′-octahydro-1,1′-binaphthyl) and BIPHEP (BIPHEP = 2,2′-bis(diphenylphosphino)-1,1′-biphenyl), to compare the behaviour of three different catalytic systems (see the Supporting Information for complete data and the related discussion). The data extracted from these experiments were analogous to those obtained with BINAP (with the only changes in the expected mass shifts arising from the different masses of the various phosphines). Therefore, the presence of the proposed species in the cycloaddition reactions was confirmed.

After the experimental detection of the intermediates, the challenge remained as to how to draw a structure for the monoyne insertion intermediate. To this end, we carried out DFT calculations to determine whether this intermediate is one of the three possible structures (**V**, **VI**, or **VII**) represented in the mechanistic proposal in Scheme 1. The reaction mechanism involving diyne **4** and alkyne **2c** with Rh/

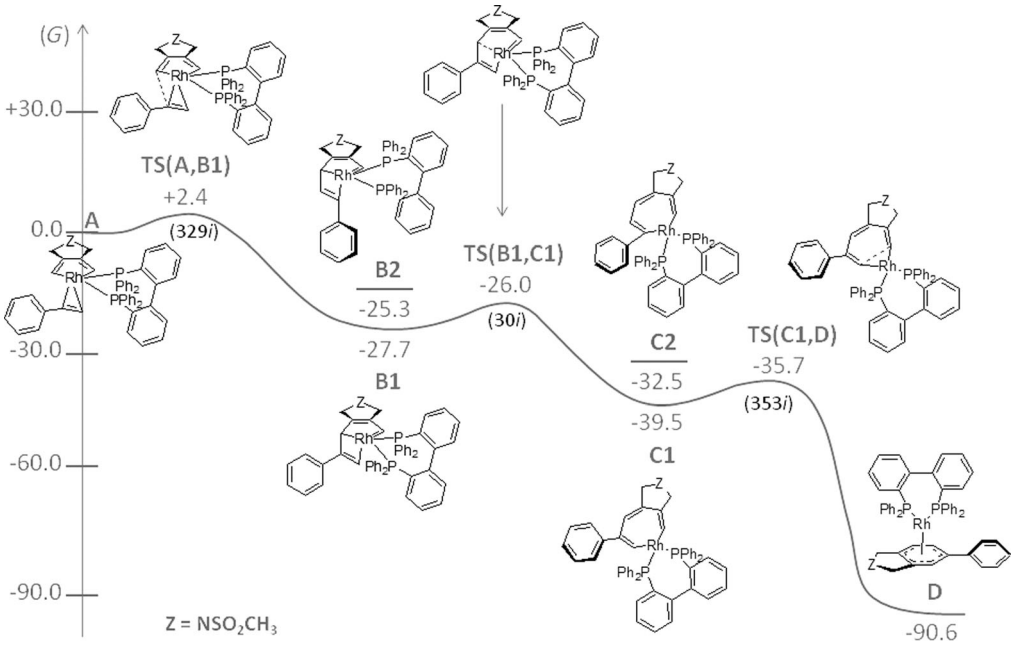

Figure 5. Gibbs energy profile (in kcal mol^{-1}) for the formation of the product **D** from **A** with Z = NSO_2CH_3.

BIPHEP as the catalytic system was studied at the B3LYP/cc-pVDZ-PP level of theory (see Computational details). To reduce the computational cost, the Ts group was replaced by an SO_2CH_3 substituent. Our simulations started from complex **A** (the π-complex between phenylacetylene **2c** and our model of the $[Rh(BIPHEP)(\mathbf{4})]^+$ species), since this is the first structure in the whole reaction mechanism with the required number and type of atoms to be the experimentally detected (intermediate $[Rh(BIPHEP)(\mathbf{4})(\mathbf{2c})]^+$). Figure 5 shows the Gibbs energy profile for the transformation of complex **A** into the final product **D**. The relative Gibbs energy of **A** with respect to $[Rh(BIPHEP)]^+$, phenylacetylene **2c**, and our model of diyne **4** is −44.8 kcal mol^{-1}. This represents the stabilization gain in Gibbs energy during the initial oxidative coupling together with the π-complexation of phenylacetylene. Subsequent formal [5+2] alkyne addition of phenylacetylene **2c** in the π-complex **A** leads to the rhodabicyclo[3.2.0]heptatriene complex **B1** (see Figures 5 and 6). Another rhodabicyclo[3.2.0]heptatriene complex **B2** could have been formed from an initial π-complexation of phenylacetylene with the phenyl group of **2c** pointing in the direction of the BIPHEP group. However, complex **B1** with the phenyl group of the phenylacetylene species pointing away from the BIPHEP substituent is more favourable than **B2** by 2.4 kcal mol^{-1} due to the lower steric repulsion and, for this reason, the reaction through intermediate **B2** was discarded. The transition state (TS) for the conversion of **A** to **B1**, TS(**A**,**B1**) has a Gibbs energy barrier of 2.4 kcal mol^{-1} and the process is exergonic by 27.7 kcal mol^{-1}. The most interesting bond lengths and angles of the molecular structure of TS(**A**,**B1**) are depicted in Figure 6. The five- and four-membered bicyclic ring **B1** evolves to the cycloheptatriene complex **C1** through the transition state TS(**B1**,**C1**) with a

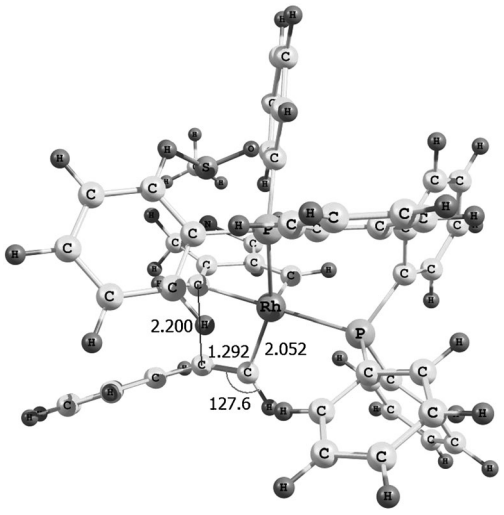

Figure 6. Optimized structure at the B3LYP level of transition state TS(**A**,**B1**) with selected bond distances (Å) and angles (°).

Gibbs energy barrier of 1.7 kcal mol^{-1} (see Figures 5 and 7).[17] This process is exergonic by 11.8 kcal mol^{-1}. Interestingly, the molecular structure of **C1** depicted in Figure 8 shows a clear bond length alternation in the rhodacycloheptatriene ring.

Intermediate **B2** could also have been transformed into **C2**. However, **C2** is 7.0 kcal mol^{-1} less stable than **C1** and it is therefore likely that the route through **C2** is not operative. In the final step, complex **D** is formed through a very exergonic reductive elimination step (51.1 kcal mol^{-1}) through TS(**C1**,**D**), which has a barrier of 2.2 kcal mol^{-1}. Finally, the dissociation of product **3c** and the recovery of the Rh^I/

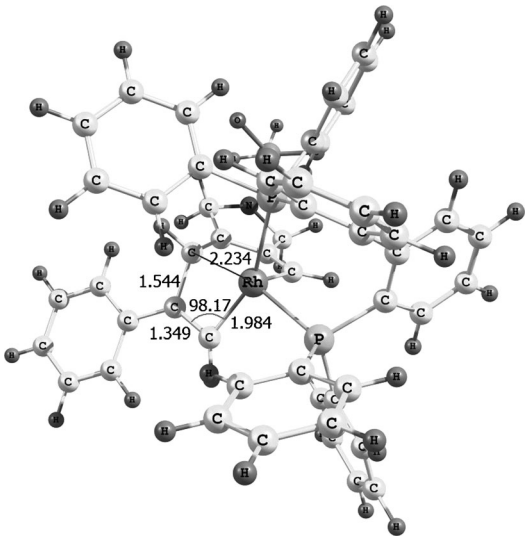

Figure 7. Optimized structure at the B3LYP level of transition state TS(**B1**,**C1**) with selected bond distances (Å) and angles (°).

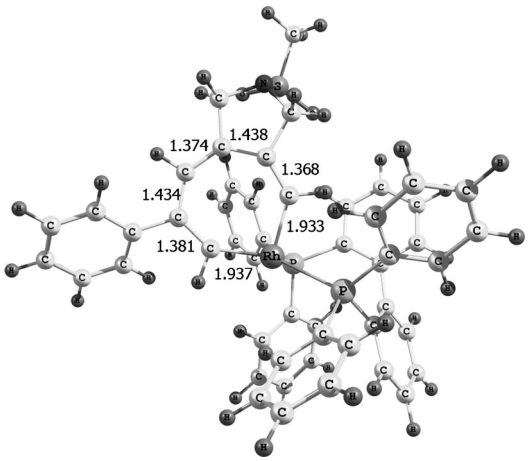

Figure 8. Optimized structure at the B3LYP level of complex **C1** with selected bond distances (Å) and angles (°).

BIPHEP catalyst from complex **D** is a slightly endergonic process that only requires 5.8 kcal mol^{-1}.

Our B3LYP/cc-pVDZ-PP results indicate that the overall cycloaddition reaction of diyne **4** and alkyne **2c** catalysed by Rh/BIPHEP is exergonic by -129.7 kcal mol^{-1}. Moreover, reaction **4**+**2c**+Rh/BIPHEP to yield **D** is exergonic by -135.5 kcal mol^{-1}. Most theoretical studies of [2+2+2] reaction mechanisms carried out to date have yielded either the rhodabicyclo[3.2.0]heptatriene or the cycloheptatriene complex. The coexistence of both in the same route is not common, although it is not unprecedented.[6c,d,l] Our simulations exclude the 7-metallanorbornadiene complex **VI** as the monoyne insertion intermediate, since it has not been possible to locate such a complex on the potential energy surface. On the other hand, our results favour the assignment of the cycloheptatriene complex **V** as the insertion intermediate since the forward barrier on the way to the products is slightly higher for **C1** than for **B1**. The small energy difference between the two Gibbs energy barriers (just 0.5 kcal mol^{-1}) prevents a definitive conclusion and the assignment of this intermediate as the rhodabicyclo[3.2.0]heptatriene complex **VII** cannot be completely excluded.

To sum up, the picture of the catalytic cycle obtained after ESI-MS and DFT calculations of the studied reactions is shown in Scheme 7. All intermediates were detected and characterized, and as an example the *m*/*z* ratios for the detected species together with their characteristic CID fragmentations are shown for the reaction between diyne **4** and phenylacetylene **2c**, using Rh^{I}/BIPHEP as the catalytic system.

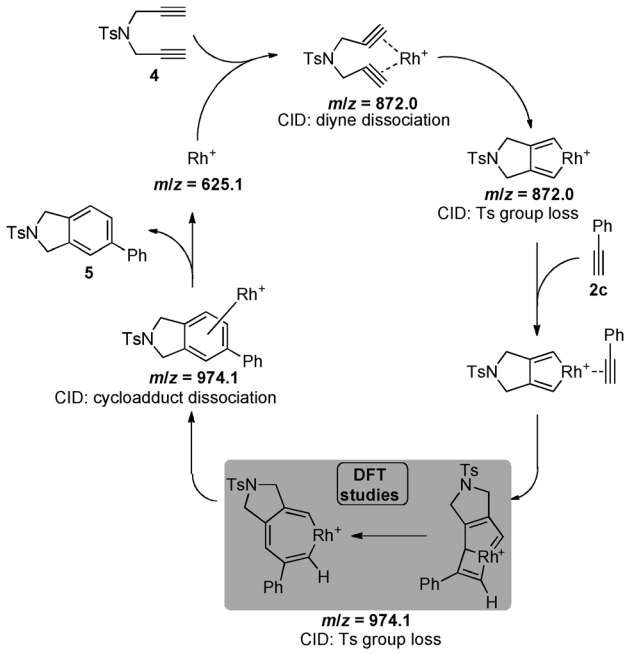

Scheme 7. Catalytic cycle proposed for the [2+2+2] cycloaddition of diynes and monoynes under Rh/bisphosphine catalysis (the BIPHEP ligand has been omitted for clarity) with detected ESI-MS species and CID characterization.

Conclusion

ESI-MS offers a fruitful approach to the analysis of reaction intermediates in the [2+2+2] cycloaddition of diynes and monoynes. The cationic nature of the reaction intermediates provided by the inherently cationic catalytic system used (BINAP/[Rh(cod)$_2$]BF$_4$), as opposed to the neutrality of the reactants and the products of the reaction, has been the key to the observation of those intermediates present in particularly low concentrations that other techniques have been unable to characterize. This has allowed the direct detection of the elusive intermediates resulting from the insertion of the monoyne into the rhodacyclopentadiene for the first time. Furthermore, this is the first time that the cationic rhodium catalyst has been investigated in a theoretical study of a [2+2+2] cycloaddition reaction. Our DFT results indicate

that the cycloheptatriene intermediate is the most likely structure for the monoyne insertion intermediate, since it has the highest forward barrier for the different steps of the analysed reaction mechanism. However, the small differences in energy barriers do not allow us to rule out the possibility of this insertion intermediate being the rhodabicyclo-[3.2.0]heptatriene complex.

Experimental Section

General: Diynes **1**[18] and **4**[19] were prepared as previously described. Compounds **3c**[4j] and **5**[9g] were prepared and characterized previously in our laboratory. Reaction mixtures were subjected to column chromatography on silica gel (230–400 mesh). ^{1}H and ^{13}C NMR spectra were recorded on Bruker 300 or 400 MHz NMR spectrometers. ^{1}H and ^{13}C chemical shifts (δ) were referenced to internal solvent resonances and are reported relative to $SiMe_4$.

ESI-MS instrument: Samples were studied in positive-ion mode with a 6000 ESI Ion Trap LC/MS (Bruker Daltonics) using nitrogen as the nebulizer gas. Pure samples such as rhodium pre-catalyst, phosphines, diyne reagents, and isolated cycloadducts were introduced as 2.5×10^{-3} M solutions in methanol into the ESI source by means of a liquid chromatographic system (HPLC P1200, Agilent) at a flow rate of 100 μL min^{-1}. The catalytic system and the aliquots sampled from the reaction mixture (100 μL in dichloromethane or dichloroethane) were analysed after dilution in methanol (1 mL at room temperature) by direct infusion into the ESI source by a syringe pump at a flow rate of 5 μL min^{-1}. The time elapsed between sampling and injection was kept below 1 min. A spray voltage of 4.5 kV, a capillary voltage of about 40 V, a drying temperature of 350 °C, and a sheath gas flow rate of 7 L min^{-1} were adjusted to ensure reasonably soft ionization. Using two octopoles, the ions were guided from the source into the ion trap for storage and manipulation in the presence of about 10^{-5} mbar helium as a trapping gas. For detection, the ions were ejected from the trap to an electron multiplier. For collision-induced-dissociation (CID) spectra, the ions were mass-selected in the ion trap and then kinetically accelerated within the helium gas present in the ion trap as the collision and cooling gas. Collision energies and window widths were chosen to provide reasonable yields of the fragmented ions while maintaining the parent ion as the most abundant one. The maximum accumulation time was in the range 50–100 ms. Mass spectra were recorded from *m/z* 200 to 1400, and seven spectral averages were accumulated to improve the signal-to-noise ratio. The isotope pattern was calculated using a Bruker Daltonics program.

General procedure for intermolecular [2+2+2] cycloaddition reactions catalysed by Rh^I-BINAP formed in situ: In a 25 mL flask, a mixture of $[Rh(cod)_2]BF_4$ (0.05 equiv) and the ligand BINAP (0.05 equiv) was dissolved in dichloromethane (3 mL). Hydrogen gas was introduced into the catalyst solution with stirring for 30 min. The resulting mixture was then concentrated to dryness, the residue was redissolved in dichloromethane or dichloroethane (0.5 mL), and the solution was stirred under an N_2 atmosphere. A solution of the alkyne (1.5 equiv) in dichloromethane or dichloroethane (0.5 mL) was then added at room temperature followed by a solution of the diyne (1 equiv) in dichloromethane or dichloroethane (1.5 mL). The reaction mixture was then stirred at room temperature or under reflux until completion (TLC monitoring). The solvent was evaporated and the residue was purified by column chromatography on silica gel.

Compound 3a: Column chromatography: hexanes/dichloromethane (1:1). Colourless solid. M.p. 150–152 °C; IR (ATR): $\tilde{\nu}$ = 2918, 1340, 1159, 1098 cm^{-1}; ^{1}H NMR (300 MHz, $CDCl_3$, 25 °C, TMS): δ = 2.05 (s, 3H), 2.18 (s, 3H), 2.38 (s, 3H), 2.41 (s, 3H), 4.61 (s, 4H), 6.92 (s, 1H), 7.09 (d, ^3J(H,H) = 8.1 Hz, 2H), 7.18 (d, ^3J(H,H) = 8.1 Hz, 2H), 7.32 (d, ^3J(H,H) = 8.4 Hz, 2H), 7.80 ppm (d, ^3J(H,H) = 8.4 Hz, 2H); ^{13}C NMR (75 MHz, $CDCl_3$, 25 °C): δ = 16.3, 18.2, 21.1, 21.5, 53.5, 53.9, 127.2, 127.6, 128.8, 129.0, 129.5, 129.8, 130.6, 133.7, 135.7, 136.6, 138.0, 141.9, 143.6 ppm; ESI-MS: *m/z*: 392.1 $[M+H]^+$, 414.1 $[M+Na]^+$, 805.1 $[2M+Na]^+$; elemental analysis calcd (%) for $[C_{24}H_{25}NO_2S\cdot0.5(C_6H_{14})]$: C 74.96, H 6.99, N 3.24; found: C 75.26, H 7.20, N 3.46.

Compound 3b: Column chromatography: hexanes/dichloromethane (1:2). Colourless solid. M.p. 128–130 °C; IR (ATR): $\tilde{\nu}$ = 2921, 2851, 1347, 1161 cm^{-1}; ^{1}H NMR (400 MHz, $CDCl_3$, 25 °C, TMS): δ = 2.06 (s, 3H), 2.19 (s, 3H), 2.42 (s, 3H), 3.84 (s, 3H), 4.62 (s, 4H), 6.91 (d, ^3J(H,H) = 8.8 Hz, 2H), 6.93 (s, 1H), 7.15 (d, ^3J(H,H) = 8.4 Hz, 2H), 7.33 (d, ^3J(H,H) = 8.8 Hz, 2H), 7.81 ppm (d, ^3J(H,H) = 8.4 Hz, 2H); ^{13}C NMR (75 MHz, $CDCl_3$, 25 °C): δ = 16.4, 18.2, 21.5, 53.5, 53.9, 55.3, 113.6, 127.3, 127.6, 129.5, 129.8, 130.3, 130.6, 133.3, 133.6, 133.8, 135.7, 141.5, 143.6, 158.6 ppm; ESI-MS: *m/z*: 430.2 $[M+Na]^+$, 446.1 $[M+K]^+$, 837.2 $[2M+Na]^+$; ESI-HRMS: calcd *m/z* for $[C_{24}H_{25}NO_3S+H]^+$ 408.1628, found 408.1643; calcd *m/z* for $[C_{24}H_{25}NO_3S+Na]^+$ 430.1447, found 430.1459.

Compound 3d: Column chromatography: hexanes/dichloromethane (1:1). Colourless solid. M.p. 203–205 °C; IR (ATR): $\tilde{\nu}$ = 2918, 1335, 1159 cm^{-1}; ^{1}H NMR (400 MHz, $CDCl_3$, 25 °C, TMS): δ = 1.35 (s, 9H), 2.08 (s, 3H), 2.19 (s, 3H), 2.42 (s, 3H), 4.62 (s, 4H), 6.95 (s, 1H), 7.15 (d, ^3J(H,H) = 8.4 Hz, 2H), 7.33 (d, ^3J(H,H) = 8.4 Hz, 2H), 7.38 (d, ^3J(H,H) = 8.4 Hz, 2H), 7.81 ppm (d, ^3J(H,H) = 8.4 Hz, 2H); ^{13}C NMR (75 MHz, $CDCl_3$, 25 °C): δ = 16.4, 18.2, 21.5, 31.4, 34.5, 53.5, 53.9, 125.0, 127.3, 127.6, 128.8, 129.4, 129.8, 130.7, 133.7, 134.0, 135.7, 137.9, 141.8, 143.6, 149.8 ppm; ESI-MS: *m/z*: 434.2 $[M+H]^+$, 456.1 $[M+Na]^+$, 472.1 $[M+K]^+$, 889.2 $[2M+Na]^+$; elemental analysis calcd (%) for $[C_{27}H_{31}NO_2S\cdot0.5(C_6H_{14})]$: C 75.91, H 7.64, N 2.95; found: C 75.68, H 7.85, N 3.34.

Compound 3e: Column chromatography: hexanes/dichloromethane (6:4). Colourless solid. M.p. 138–140 °C; IR (ATR): $\tilde{\nu}$ = 2935, 1345, 1221, 1163 cm^{-1}; ^{1}H NMR (400 MHz, $CDCl_3$, 25 °C, TMS): δ = 2.03 (s, 3H), 2.19 (s, 3H), 2.42 (s, 3H), 4.61 (s, 4H), 6.91 (s, 1H), 7.07 (dd, ^3J(H,H) = 8.8 Hz, ^3J(H,F) = 8.8 Hz, 2H), 7.18 (dd, ^3J(H,H) = 8.8 Hz, ^4J(H,F) = 5.6 Hz, 2H), 7.33 (d, ^3J(H,H) = 8.0 Hz, 2H), 7.80 ppm (d, ^3J(H,H) = 8.0 Hz, 2H); ^{13}C NMR (75 MHz, $CDCl_3$, 25 °C): δ = 16.3, 18.2, 21.5, 53.4, 53.8, 115.0 (d, ^2J(C,F) = 21.0 Hz), 127.2, 127.6, 129.6, 129.9, 130.5, 130.7 (d, ^3J(C,F) = 6.7 Hz), 133.8, 134.1, 135.8, 136.8 (d, ^4J(C,F) = 3.7 Hz), 140.8, 143.7, 161.9 ppm (d, ^1J(C,F) = 245 Hz); ESI-MS: *m/z*: 418.2 $[M+Na]^+$, 434.1 $[M+K]^+$, 813.1 $[2M+Na]^+$; ESI-HRMS: calcd *m/z* for $[C_{23}H_{22}FNO_2S+H]^+$ 396.1428, found 396.1429; calcd *m/z* for $[C_{23}H_{22}FNO_2S+Na]^+$ 418.1247, found 418.1246.

Compound 3f: Column chromatography: hexanes/dichloromethane (1:1). Colourless solid. M.p. 61–63 °C; IR (ATR): $\tilde{\nu}$ = 2920, 1340, 1158 cm^{-1}; ^{1}H NMR (300 MHz, $CDCl_3$, 25 °C, TMS): δ = 2.03 (s, 3H), 2.19 (s, 3H), 2.42 (s, 3H), 4.61 (s, 4H), 6.90 (s, 1H), 7.09 (d, ^3J(H,H) = 8.5 Hz, 2H), 7.33 (d, ^3J (H,H) = 8.5 Hz, 2H), 7.51 (d, ^3J(H,H) = 8.4 Hz, 2H), 7.81 ppm (d, ^3J(H,H) = 8.4 Hz, 2H); ^{13}C NMR (75 MHz, $CDCl_3$, 25 °C): δ = 16.6, 18.5, 21.8, 53.8, 54.2, 121.5, 127.4, 127.9, 130.1, 130.2, 130.7, 131.2, 131.6, 134.3, 134.7, 136.3, 140.2, 140.9, 144.0 ppm; ESI-MS: *m/z*: 456–458 $[M+H]^+$, 478–480 $[M+Na]^+$, 494–496 $[M+K]^+$, 935 $[2M+Na]^+$; elemental analysis calcd (%) for $[C_{23}H_{22}NO_2SBr\cdot(C_6H_{14})]$: C 64.68, H 5.99, N 2.60; found: C 63.92, H 6.26, N 2.68.

Compound 7: Column chromatography: hexanes/ethyl acetate (9:1). Yellow solid. M.p. 72–74 °C; IR (ATR): $\tilde{\nu}$ = 2922, 1729, 1241, 1185, 1067 cm^{-1}; ^{1}H NMR (300 MHz, $CDCl_3$, 25 °C, TMS): δ = 1.26 (t, J = 7.2 Hz, 6H), 2.38 (s, 3H), 3.62 (d, J = 6 Hz, 4H), 4.21 (q, J = 7.2 Hz, 4H), 7.20–7.25 (m, 3H), 7.37 (d, ^3J(H,H) = 8.1 Hz, 2H), 7.44 ppm (d, ^3J(H,H) = 8.1 Hz, 2H); ^{13}C NMR (75 MHz, $CDCl_3$, 25 °C): δ = 14.4, 21.4, 60.8, 62.1, 123.1, 124.7, 126.3, 127.3, 129.7, 137.1, 138.7, 139.2, 140.6, 141.0, 172.0 ppm; ESI-MS: *m/z*: 353.2 $[M+H]^+$, 375.2 $[M+Na]^+$, 727.3 $[2M+Na]^+$.

Computational details: All geometry optimizations were performed without symmetry constraints using the hybrid DFT B3LYP[20] method with the Gaussian 03[21] program package. Analytical Hessians were computed to determine the nature of stationary points (one or zero imaginary frequencies for transition states and minima, respectively) and to calculate unscaled zero-point energies (ZPEs) as well as thermal corrections and entropy effects using the standard statistical mechanics relationships for an ideal gas.[22] The latter two terms were computed at 298.15 K and 1 atm to provide the reported relative Gibbs free energies (ΔG_{298}). Fur-

thermore, the connectivity between stationary points was established by intrinsic reaction path[23] calculations. The all-electron cc-pVDZ basis set was used for P, O, N, C, S, and H atoms,[24] while for Rh we employed the cc-pVDZ-PP basis set[25] containing an effective core relativistic pseudopotential. Relative energies were computed taking into account the total number of molecules present. The Ar group of the Ts (SO_2–Ar) moiety present in the experimental diyne **4** was substituted by a CH_3 group to reduce the computational cost of the calculations.

Acknowledgements

Financial support from the Spanish Ministry of Education and Science (MEC) (Projects Nos.: CTQ2011–23121/BQU and CTQ2011–23156/BQU) and the DIUE of the Generalitat de Catalunya (Project No.: 2009SGR637) is gratefully acknowledged. M.P. thanks the Generalitat de Catalunya for a predoctoral grant. We would also like to thank Anna Costa for her technical assistance with the ESI mass spectrometer and Jesús Orduna for helpful discussions. Excellent service by the Centre de Serveis Científics i Acadèmics de Catalunya (CESCA) is gratefully acknowledged. Support for the research of M.S. was received through the ICREA Academia 2009 prize for excellence in research funded by the DIUE of the Generalitat de Catalunya.

[1] R. B. Cole, *Electrospray Ionization Mass Spectrometry - Fundamentals, Instrumentation and Applications*, Wiley, New York, **1997**.

[2] For selected reviews and monographs, see: a) D. Plattner, *Int. J. Mass Spectrom.* **2001**, *207*, 125–144; b) P. Chen, *Angew. Chem.* **2003**, *115*, 2938–2954; *Angew. Chem. Int. Ed.* **2003**, *42*, 2832–2847; c) L. S. Santos, L. Knaack, J. O. Metzger, *Int. J. Mass Spectrom.* **2005**, *246*, 84–104; d) M. N. Eberlin, *Eur. J. Mass Spectrom.* **2007**, *13*, 19–28; e) L. S. Santos, *Reactive Intermediates - MS Investigations in Solution*, Wiley-VCH, Weinheim, **2010**; f) J. Roithová, *Chem. Soc. Rev.* **2012**, *41*, 547–559.

[3] For recent and selected references, see: a) H.-Y. Wang, W.-L. Yim, T. Klüner, J. O. Metzger, *Chem. Eur. J.* **2009**, *15*, 10948–10959; b) C. A. Müller, C. Markert, A. M. Teichert, A. Pfaltz, *Chem. Commun.* **2009**, 1607–1618; c) M. A. Schade, J. E. Fleckenstein, P. Knochel, K. Koszinowski, *J. Org. Chem.* **2010**, *75*, 6848–6857; d) T. A. Fernandes, B. G. Vaz, M. N. Eberlin, A. J. M. da Silva, P. R. R. Costa, *J. Org. Chem.* **2010**, *75*, 7085–7091; e) C. H. Beierlein, B. Breit, R. A. P. Schmidt, D. A. Plattner, *Organometallics* **2010**, *29*, 2521–2532; f) D. Agrawal, D. Schröder, C. M. Frech, *Organometallics* **2011**, *30*, 3579–3587; g) D. Agrawal, D. Schröder, *Organometallics* **2011**, *30*, 32–35; h) M. A. Henderson, J. Luo, A. Oliver, J. S. McIndoe, *Organometallics* **2011**, *30*, 5471–5479; i) K. L. Vikse, Z. Ahmadi, C. C. Manning, D. A. Harrington, J. S. McIndoe, *Angew. Chem.* **2011**, *123*, 8454–8456; *Angew. Chem. Int. Ed.* **2011**, *50*, 8304–8306; j) H.-Y. Wang, W.-L. Yim, Y.-L. Guo, J. O. Metzger, *Organometallics* **2012**, *31*, 1627–1634.

[4] For previous ESI-MS studies from our group, see: a) M. A. Aramendía, F. Lafont, M. Moreno-Mañas, R. Pleixats, A. Roglans, *J. Org. Chem.* **1999**, *64*, 3592–3594; b) M. Moreno-Mañas, R. Pleixats, J. Spengler, C. Chevrin, B. Estrine, S. Bouquillon, F. Hénin, J. Muzart, A. Pla-Quintana, A. Roglans, *Eur. J. Org. Chem.* **2003**, 274–283; c) J. Masllorens, M. Moreno-Mañas, A. Pla-Quintana, A. Roglans, *Org. Lett.* **2003**, *5*, 1559–1561; d) C. Chevrin, J. Le Bras, F. Hénin, J. Muzart, A. Pla-Quintana, A. Roglans, R. Pleixats, *Organometallics* **2004**, *23*, 4796–4799; e) J. Comelles, M. Moreno-Mañas, E. Pérez, A. Roglans, R. M. Sebastián, A. Vallribera, *J. Org. Chem.* **2004**, *69*, 6834–6842; f) A. Pla-Quintana, A. Roglans, *ARKIVOC* **2005**, *ix*, 51–62; g) J. Masllorens, I. González, A. Roglans, *Eur. J. Org. Chem.* **2007**, 158–166; h) J. Comelles, A. Pericas, M. Moreno-Mañas, A. Vallribera, G. Drudis-Solé, A. Lledós, T. Parella, A. Roglans, S. García-Granda, L. Roces-Fernández, *J. Org. Chem.* **2007**, *72*, 2077–2087; i) C. Chevrin, J. Le Bras, A. Roglans, D. Harakat, J. Muzart, *New J. Chem.* **2007**, *31*, 121–126; j) I. González, A. Pla-Quintana, A. Roglans, *Synlett* **2009**, 2844–2848; k) A. Dachs, A. Torrent, A. Pla-Quintana, A. Roglans, A. Jutand, *Organometallics* **2009**, *28*, 6036–6043; l) J. Salabert, R. M. Sebastián, A. Vallribera, A. Roglans, C. Nájera, *Tetrahedron* **2011**, *67*, 8659–8664.

[5] N. E. Schore, *Chem. Rev.* **1988**, *88*, 1081–1119.

[6] For a pioneering semiempirical study, see: a) C. Bianchini, K. G. Caulton, C. Chardon, M.-L. Doublet, O. Eisenstein, S. A. Jackson, T. J. Johnson, A. Meli, M. Peruzzini, W. E. Streib, A. Vacca, F. Vizza, *Organometallics* **1994**, *13*, 2010–2023. For DFT studies of the mechanism for alkyne cyclotrimerization, see: b) J. H. Hardesty, J. B. Koerner, T. A. Albright, G.-Y. Lee, *J. Am. Chem. Soc.* **1999**, *121*, 6055–6067; c) K. Kirchner, M. J. Calhorda, R. Schmid, L. F. Veiros, *J. Am. Chem. Soc.* **2003**, *125*, 11721–11729; d) Y. Yamamoto, T. Arakawa, R. Ogawa, K. Itoh, *J. Am. Chem. Soc.* **2003**, *125*, 12143–12160; e) R. Schmid, K. Kirchner, *Eur. J. Inorg. Chem.* **2004**, 2609–2626; f) A. A. Dahy, N. Koga, *Bull. Chem. Soc. Jpn.* **2005**, *78*, 781–791; g) A. A. Dahy, C. H. Suresh, N. Koga, *Bull. Chem. Soc. Jpn.* **2005**, *78*, 792–803; h) N. Agenet, V. Gandon, K. P. C. Vollhardt, M. Malacria, C. Aubert, *J. Am. Chem. Soc.* **2007**, *129*, 8860–8871; i) L. Orian, J. N. P. van Stralen, F. M. Bickelhaupt, *Organometallics* **2007**, *26*, 3816–3830; j) K. Kirchner, *Monatsh. Chem.* **2008**, *139*, 337–348; k) A. Dachs, A. Torrent, A. Roglans, T. Parella, S. Osuna, M. Solà, *Chem. Eur. J.* **2009**, *15*, 5289–5300; l) A. Dachs, S. Osuna, A. Roglans, M. Solà, *Organometallics* **2010**, *29*, 562–569; m) R. Xu, P. Winget, T. Clark, *Eur. J. Inorg. Chem.* **2008**, 2874–2883. For a review, see: n) J. A. Varela, C. Saá, *J. Organomet. Chem.* **2009**, *694*, 143–149.

[7] a) E. Müller, *Synthesis* **1974**, 761–774; b) M. Iglesias, C. del Pino, J. Ros, S. García Blanco, S. M. Carrera, *J. Organomet. Chem.* **1980**, *338*, 89–102; c) C. Bianchini, K. G. Caulton, C. Chardon, O. Eisenstein, K. Folting, T. J. Johnson, A. Meli, M. Peruzzini, D. J. Rauscher, W. E. Streib, F. Vizza, *J. Am. Chem. Soc.* **1991**, *113*, 5127–5129; d) H. Nishiyama, E. Niwa, T. Inoue, Y. Ishima, K. Aoki, *Organometallics* **2002**, *21*, 2572–2574; e) H. Uchimura, J.-i. Ito, S. Iwasa, H. Nishiyama, *J. Organomet. Chem.* **2007**, *692*, 481–486.

[8] V. M. Williams, J. R. Kong, B. J. Ko, Y. Mantri, J. S. Brodbelt, M.-H. Baik, M. J. Krische, *J. Am. Chem. Soc.* **2009**, *131*, 16054–16062.

[9] a) A. Pla-Quintana, A. Roglans, A. Torrent, M. Moreno-Mañas, J. Benet-Buchholz, *Organometallics* **2004**, *23*, 2762–2767; b) A. Torrent, I. González, A. Pla-Quintana, A. Roglans, M. Moreno-Mañas, T. Parella, J. Benet-Buchholz, *J. Org. Chem.* **2005**, *70*, 2033–2041; c) I. González, S. Bouquillon, A. Roglans, J. Muzart, *Tetrahedron Lett.* **2007**, *48*, 6425–6428; d) S. Brun, L. Garcia, I. González, A. Torrent, A. Dachs, A. Pla-Quintana, T. Parella, A. Roglans, *Chem. Commun.* **2008**, 4339–4341; e) L. Garcia, A. Pla-Quintana, A. Roglans, *Org. Biomol. Chem.* **2009**, *7*, 5020–5027; f) L. Garcia, A. Pla-Quintana, A. Roglans, T. Parella, *Eur. J. Org. Chem.* **2010**, 3407–3415; g) S. Brun, M. Parera, A. Pla-Quintana, A. Roglans, T. León, T. Achard, J. Solà, X. Verdaguer, A. Riera, *Tetrahedron* **2010**, *66*, 9032–9040; h) S. Brun, A. Torrent, A. Pla-Quintana, A. Roglans, X. Fontrodona, J. Benet-Buchholz, T. Parella, *Organometallics* **2012**, *31*, 318–326.

[10] For representative examples, see: a) K. Tanaka, *Synlett* **2007**, 1977–1993; b) K. Tanaka, *Chem. Asian J.* **2009**, *4*, 508–518; c) T. Shibata, K. Tsuchikama, *Org. Biomol. Chem.* **2008**, *6*, 1317–1323.

[11] Hydrogenation of the catalytic mixture is a usual procedure for the activation of the catalyst (see, for instance, the references cited in the reviews in ref. [10]).

[12] We postulate that MeOH is not only a better suited solvent for ESI-MS but that it also helps to stabilize the short-lived intermediates by forming solvent adducts (see, for instance, Figure S41 in the Supporting Information) or complexes which can then be split in the ESI source, thus facilitating their detection by mass spectrometry. Methanol has been shown not to have a deleterious effect on the reaction since the cycloaddition of diyne **1** and phenylacetylene **2a** (Scheme 2) works satisfactorily (75% conversion in 5 h at reflux) when run in a mixture of DCE/MeOH (1:10, *v*/*v*).

[13] a) N. Hu, Y.-P. Tu, K. Jiang, Y. Pan, *J. Org. Chem.* **2010**, *75*, 4244–4250; b) G. Xu, T. Huang, J. Zhang, J. K. Huang, T. Carlson, S.

Miao, *Rapid Commun. Mass Spectrom.* **2010**, *24*, 321–327; c) W. L. Fitch, L. He, Y.-P. Tu, L. Alexandrova, *Rapid Commun. Mass Spectrom.* **2007**, *21*, 1661–1668; d) E. M. Thurman, I. Ferrer, O. J. Pozo, J. V. Sancho, F. Hernandez, *Rapid Commun. Mass Spectrom.* **2007**, *21*, 3855–3868.

[14] The alkyne insertion intermediate has been drawn as the rhodacycloheptatriene in accordance with the results obtained by DFT calculations.

[15] Heterolytic cleavage leading to Ts loss as a neutral molecule was also observed for cycloadduct **3a**; see the Supporting Information for CID spectra of **3a**, **4**, and **5**.

[16] It should be noted that the peaks of oxidized species were much more intense in the case of the malonate-tethered diyne than for the NTs-tethered diynes.

[17] TS(**B1**,**C1**) has two imaginary frequencies at 30i and 11i. The first has the expected motion for the transformation from **B1** to **C1**. The second corresponds to a movement of a phenyl group and is likely to be the result of a numerical artifact of the quadrature grid used in the DFT calculations.

[18] M. Nishida, H. Shiga, M. Mori, *J. Org. Chem.* **1998**, *63*, 8606–8608.

[19] J. E. Brumwell, N. S. Simpkins, N. K. Terrett, *Tetrahedron Lett.* **1993**, *34*, 1219–1222.

[20] a) A. D. Becke, *J. Chem. Phys.* **1993**, *98*, 5648–5652; b) C. Lee, W. Yang, R. G. Parr, *Phys. Rev. B* **1988**, *37*, 785–789; c) P. J. Stephens, F. J. Devlin, C. F. Chabalowski, M. J. Frisch, *J. Phys. Chem.* **1994**, *98*, 11623–11627.

[21] M. J. Frisch, G. W. Trucks, H. B. Schlegel, G. E. Scuseria, M. A. Robb, J. R. Cheeseman, J. A. Montgomery Jr., T. Vreven, K. N. Kudin, J. C. Burant, J. M. Millam, S. S. Iyengar, J. Tomasi, V. Barone, B. Mennucci, M. Cossi, G. Scalmani, N. Rega, G. A. Petersson, H. Nakatsuji, M. Hada, M. Ehara, K. Toyota, R. Fukuda, J. Hasegawa, M. Ishida, T. Nakajima, Y. Honda, O. Kitao, H. Nakai, M. Klene, X. Li, J. E. Knox, H. P. Hratchian, J. B. Cross, V. Bakken, C. Adamo, J. Jaramillo, R. Gomperts, R. E. Stratmann, O. Yazyev, A. J. Austin, R. Cammi, C. Pomelli, J. W. Ochterski, P. Y. Ayala, K. Morokuma, G. A. Voth, P. Salvador, J. J. Dannenberg, G. Zakrzewski, S. Dapprich, A. D. Daniels, M. C. Strain, O. Farkas, D. K. Malick, A. D. Rabuck, K. Raghavachari, J. B. Foresman, J. V. Ortiz, Q. Cui, A. G. Baboul, S. Clifford, J. Cioslowski, B. B. Stefanov, G. Liu, A. Liashenko, P. Piskorz, I. Komaromi, R. L. Martin, D. J. Fox, T. Keith, M. A. Al-Laham, C. Y. Peng, A. Nanayakkara, M. Challacombe, P. M. W. Gill, B. Johnson, W. Chen, M. W. Wong, C. Gonzalez, J. A. Pople in Gaussian 03, Revision C.01, Gaussian, Inc., Pittsburgh, PA, **2003**.

[22] P. Atkins, J. De Paula, *Physical Chemistry*, Oxford University Press, Oxford, **2006**.

[23] C. Gonzalez, H. B. Schlegel, *J. Chem. Phys.* **1989**, *90*, 2154–2161.

[24] a) T. H. Dunning Jr., *J. Chem. Phys.* **1989**, *90*, 1007–1023; b) D. E. Woon, T. H. Dunning Jr., *J. Chem. Phys.* **1993**, *98*, 1358–1371.

[25] K. A. Peterson, D. Figgen, M. Dolg, H. Stoll, *J. Chem. Phys.* **2007**, *126*, 124101.

Received: March 15, 2012
Revised: July 3, 2012
Published online: August 30, 2012

